

Supporting Information

Polysiloxanes Bearing Pendant Redox-Active Dendritic Wedges Containing Ferrocenyl and (η^6 -Aryl)tricarbonylchromium Moieties

Magdalena Zamora, Sonia Bruña, Beatriz Alonso and Isabel Cuadrado*

Departamento de Química Inorgánica, Facultad de Ciencias, Universidad Autónoma de Madrid,
Cantoblanco, 29049, Madrid, Spain. E-mail: isabel.cuadrado@uam.es

1. Structural Characterization of Model Compounds 5 – 7	2
Figures S1 and S2: ^1H NMR and ^{13}C NMR spectra of 5	2
Figures S3 and S4: ^{29}Si NMR and IR spectra of 5	3
Figure S5: Mass spectrometry characterization by FAB for compound 5	4
Figures S6 and S7: ^1H NMR and ^{13}C NMR spectra of 6	5
Figures S8 and S9: ^{29}Si NMR and IR spectra of 6	6
Figure S10: Mass spectrometry characterization by FAB for compound 6	7
Figures S11 and S12: ^1H NMR and ^{13}C NMR spectra of 7	8
Figures S13 and S14: { ^1H – ^{29}Si } HMBC and IR spectra of 7	9
Figure S15: Mass spectrometry characterization by MALDI for compound 7	10
2. Structural Characterization of Polymers 8 – 13	11
Figures S16 and S17: ^1H NMR and ^{13}C NMR spectra of 8	11
Figures S18 and S19: { ^1H – ^{29}Si } HMBC and IR spectra of 8	12
Figures S20 and S21: ^1H NMR and ^{13}C NMR spectra of 9	13
Figures S22 and S23: ^{29}Si NMR and IR spectra of 9	14
Figures S24 and S25: ^1H NMR and ^{13}C NMR spectra of 10	15
Figures S26 and S27: ^{29}Si NMR and IR spectra of 10	16
Figures S28 and S29: ^1H NMR and ^{13}C NMR spectra of 11	17
Figures S30 and S31: ^{29}Si NMR and IR spectra of 11	18
Figures S32 and S33: ^1H NMR and IR spectra of 12	19
Figures S34 and S35: ^1H NMR and IR spectra of 13	20
3. Electrochemistry of Compounds 5–13.	21
Figure S36: CV of 7 in CH_2Cl_2	21
Figure S37: CVs of 8 in CH_2Cl_2 at different scan rates	21
Figure S38: CV responses of a carbon electrode modified with a film of 8	22
Figure S39: CV response of a platinum electrode modified with a film of 9	22
Figure S40: CV of 11 in CH_2Cl_2	23
Figure S41: CV of 13 in CH_2Cl_2	23
4. Energy-dispersive X-ray (EDX) analyses of ceramic residues	24

1.- Structural Characterization of Model Compounds 5–7

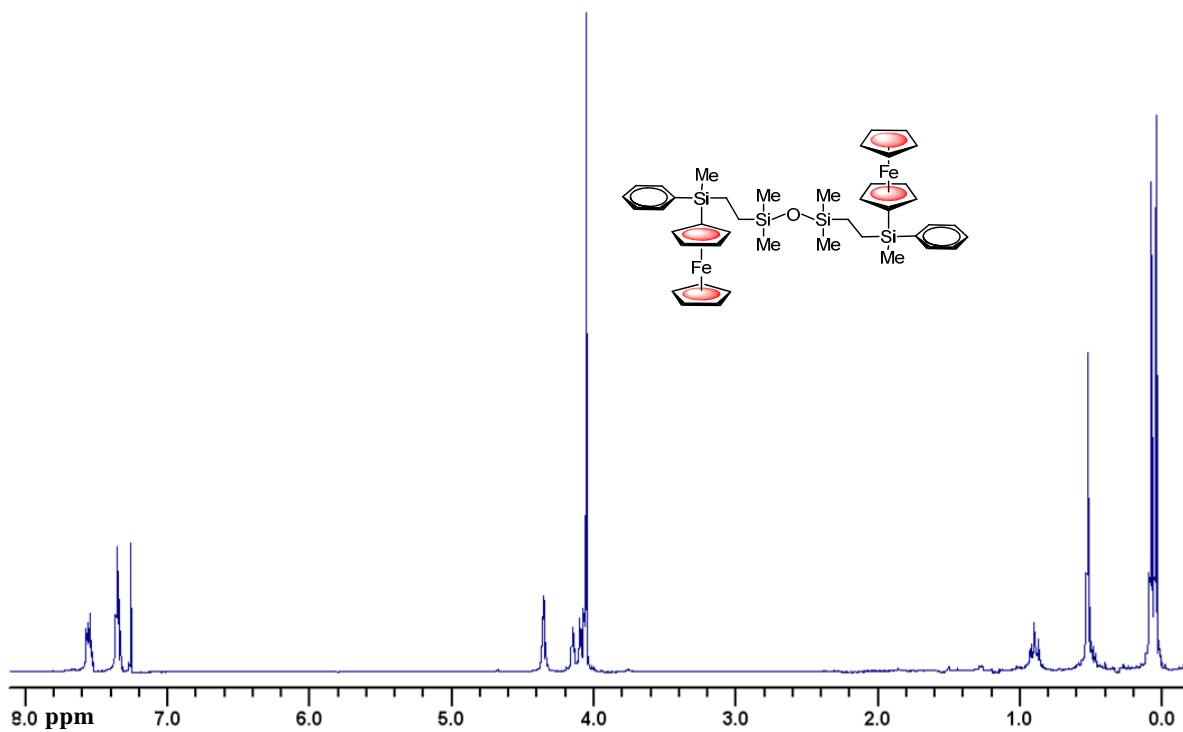


Figure S1. ¹H NMR spectrum (in CDCl₃, 300 MHz) of compound 5.

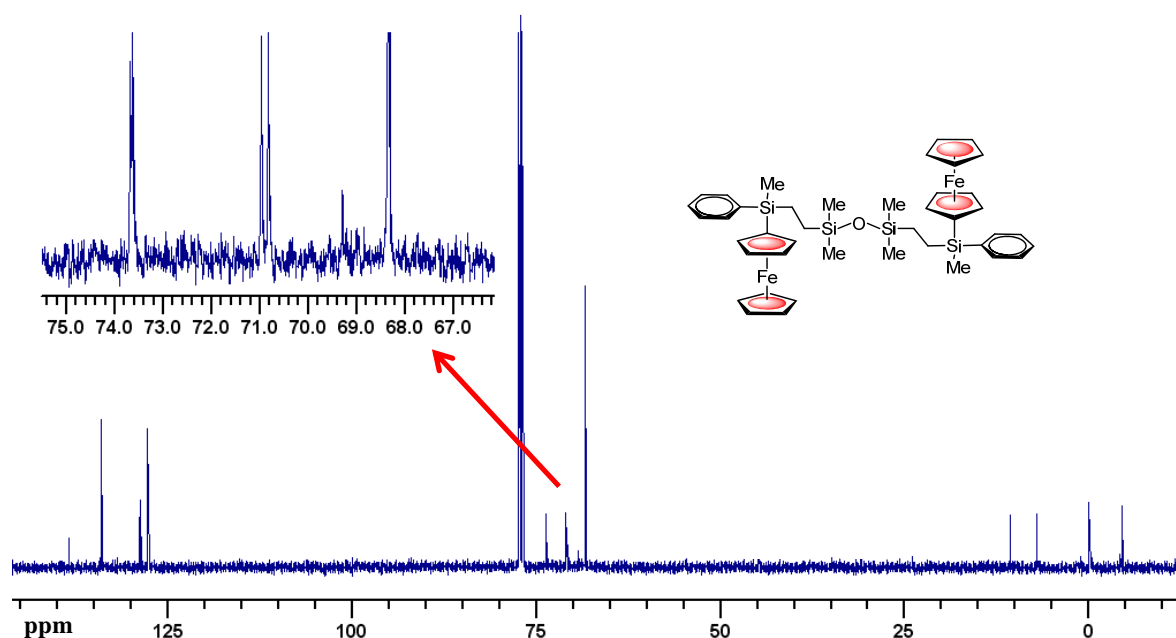


Figure S2. ¹³C NMR spectrum (in CDCl₃, 125 MHz) of compound 5 (inset: expanded view of cyclopentadienyl region).

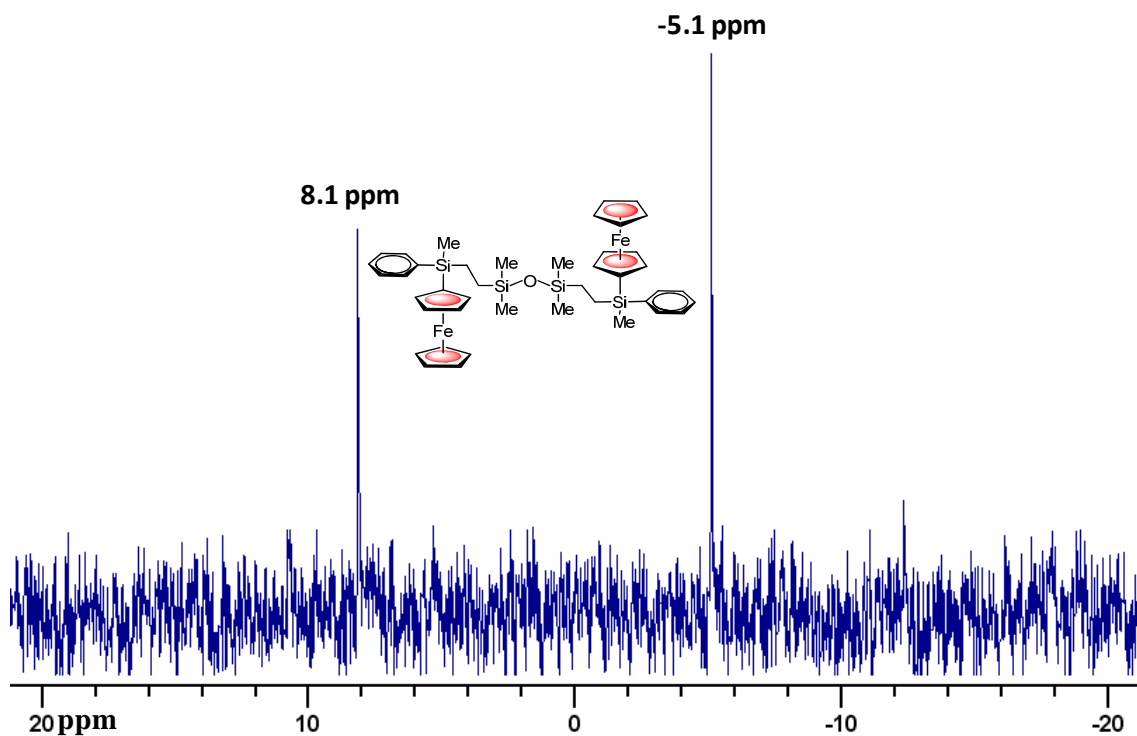


Figure S3. ^{29}Si NMR spectrum (in CDCl_3 , 99 MHz) of compound 5.

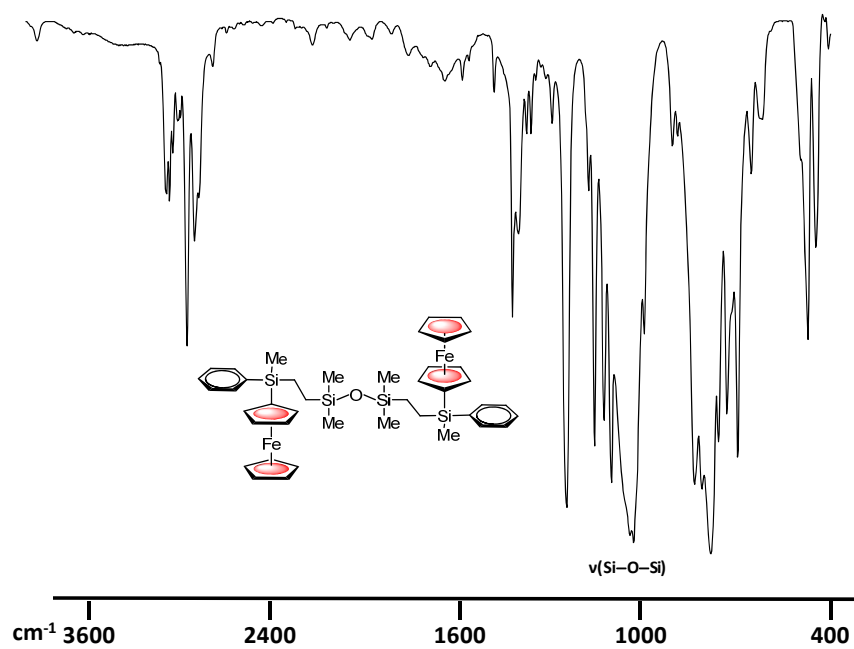


Figure S4. IR spectrum (in KBr windows) of compound 5.

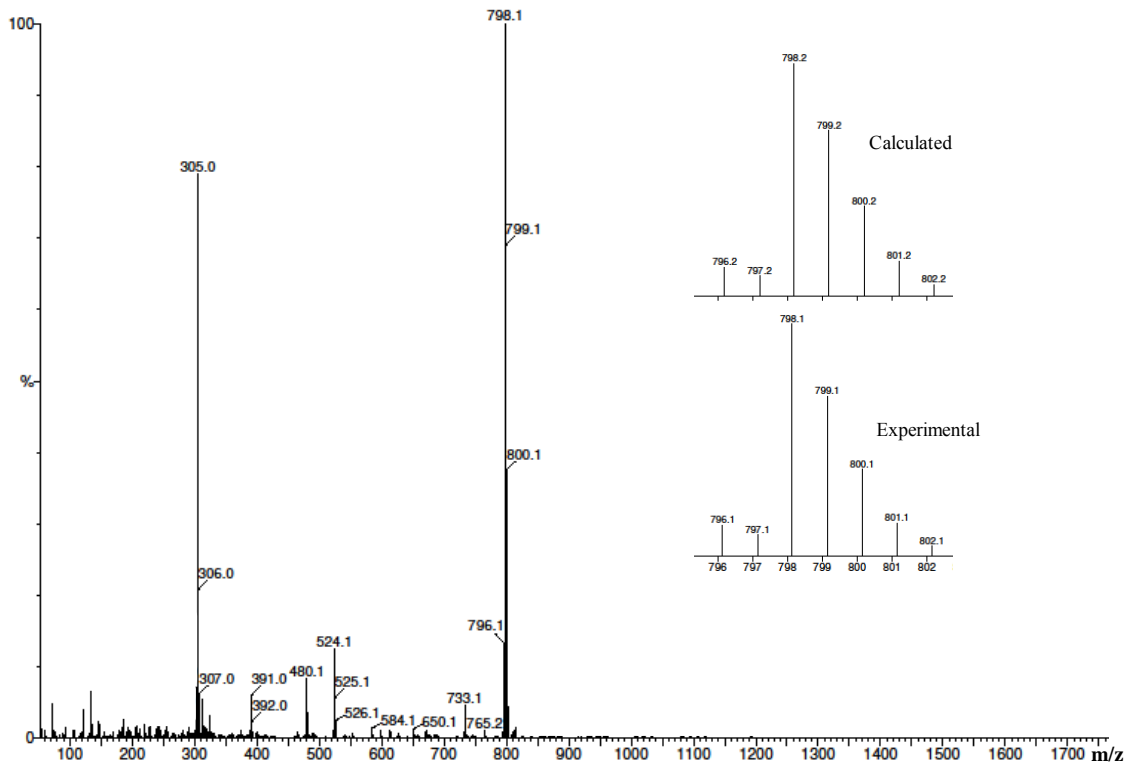


Figure S5. Mass spectrometry characterization by FAB for compound **5**. Inset: isotopic distribution of molecular ion peak of **5**.

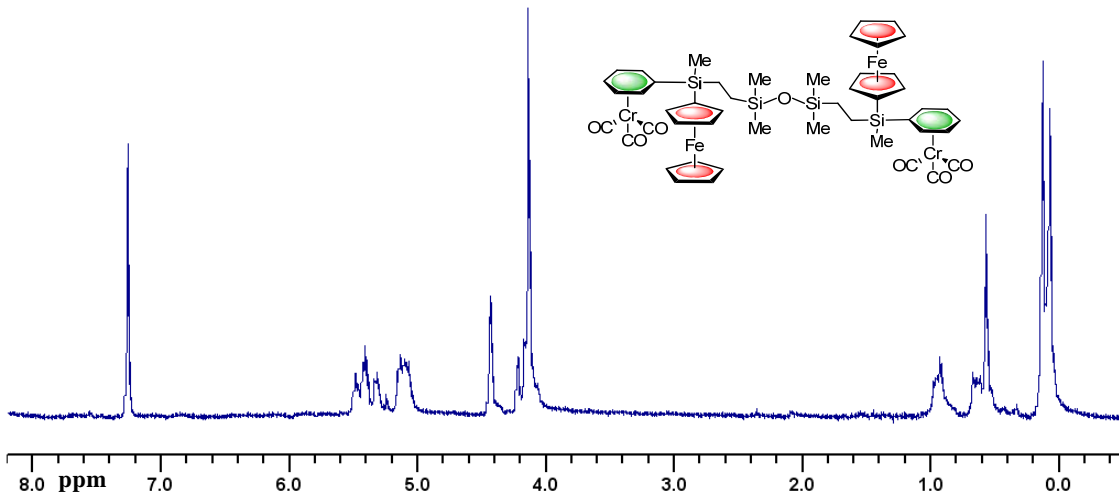


Figure S6. ^1H NMR spectrum (in CDCl_3 , 300 MHz) of compound 6.

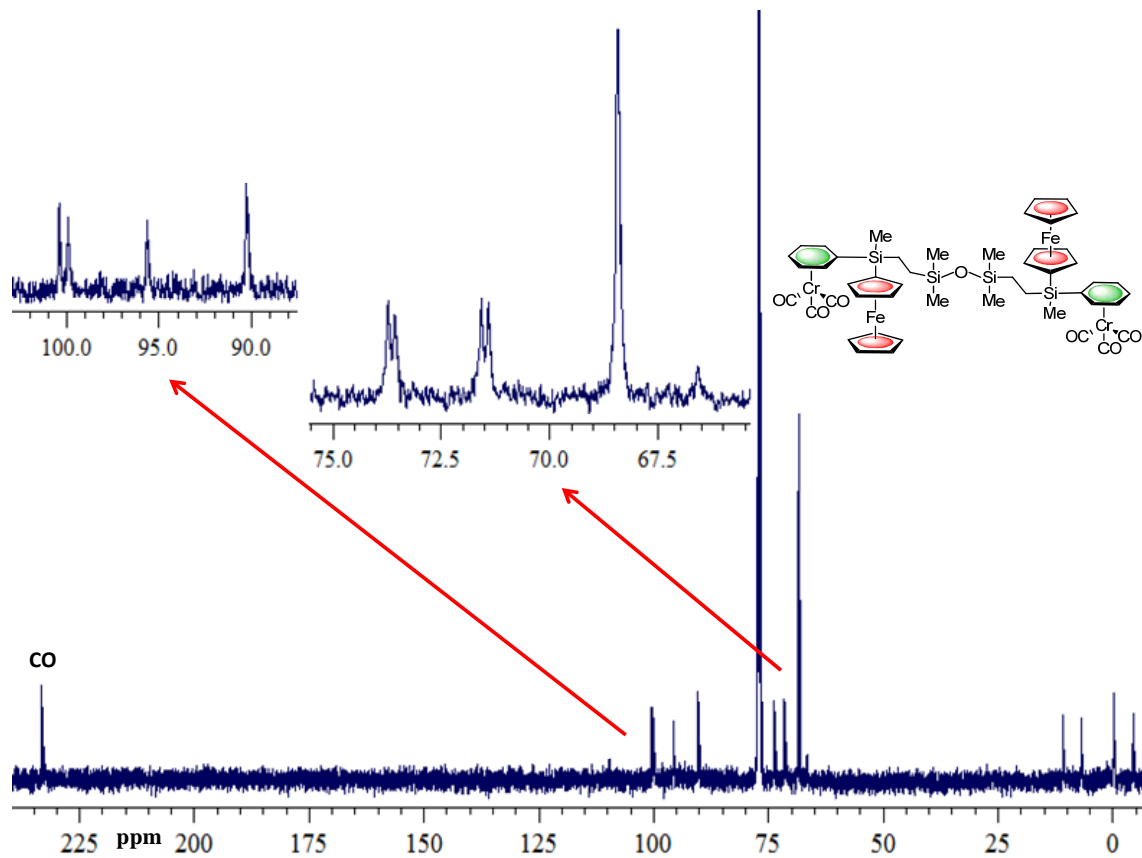


Figure S7. ^{13}C NMR spectrum (in CDCl_3 , 125 MHz) of compound 6, (inset: expanded view of phenyl and cyclopentadienyl regions).

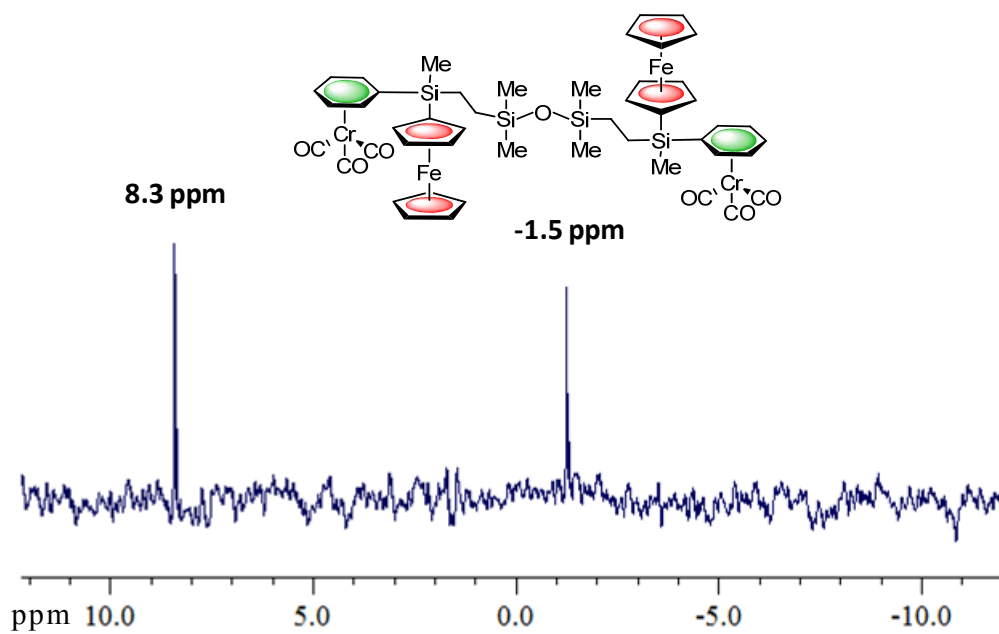


Figure S8. ²⁹Si NMR spectrum (in CDCl₃, 99 MHz) of compound 6.

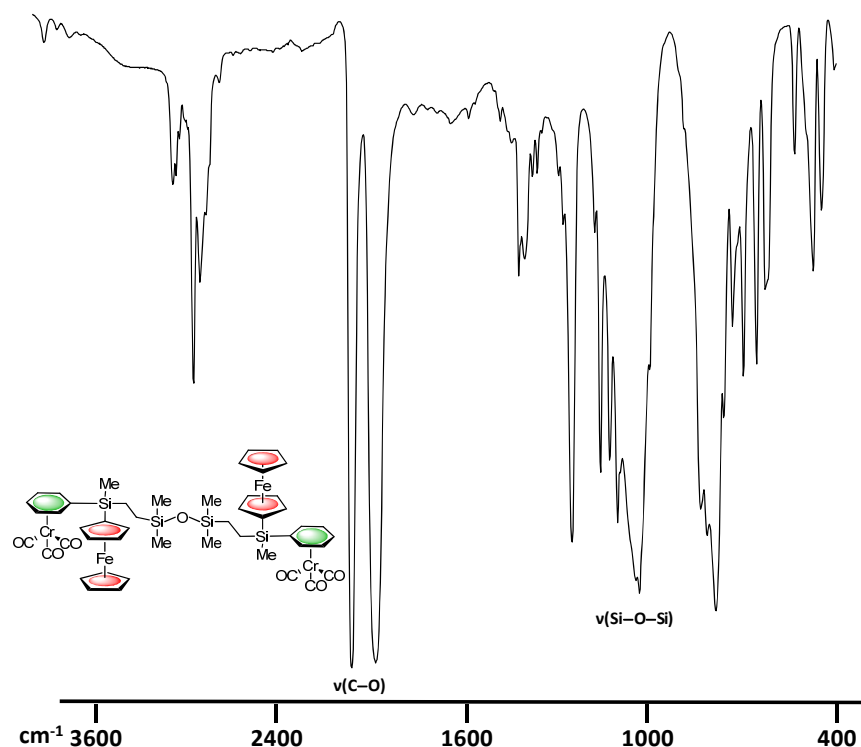


Figure S9. IR spectrum (in KBr windows) of compound 6.

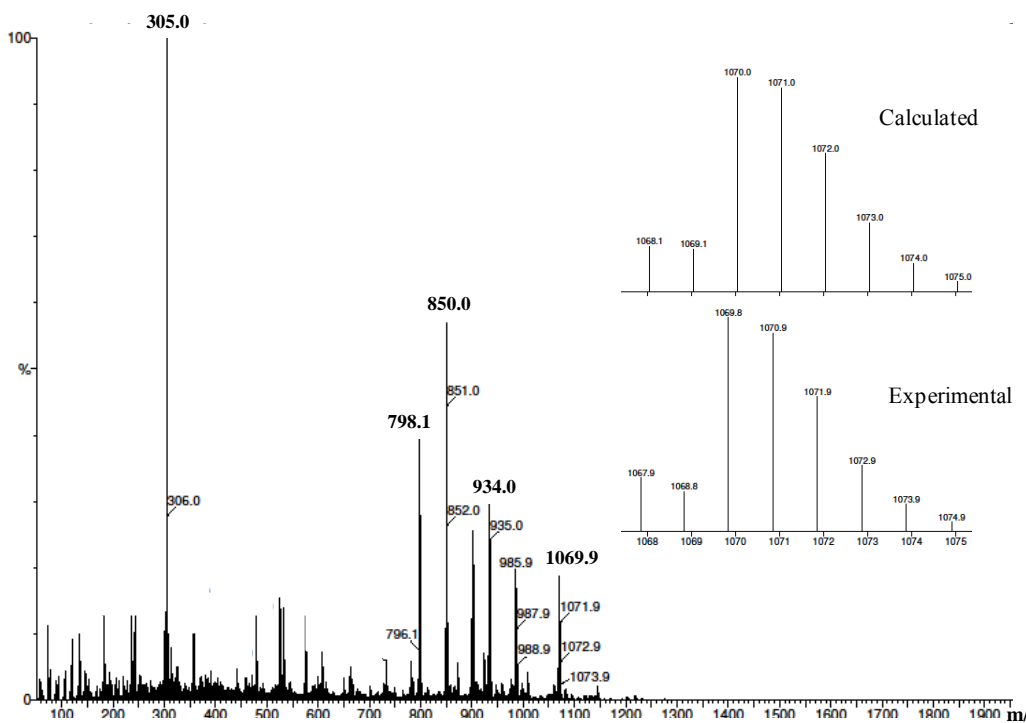


Figure S10. Mass spectrometry characterization by FAB for compound **6**. Inset: isotopic distribution of molecular ion peak of **6**.

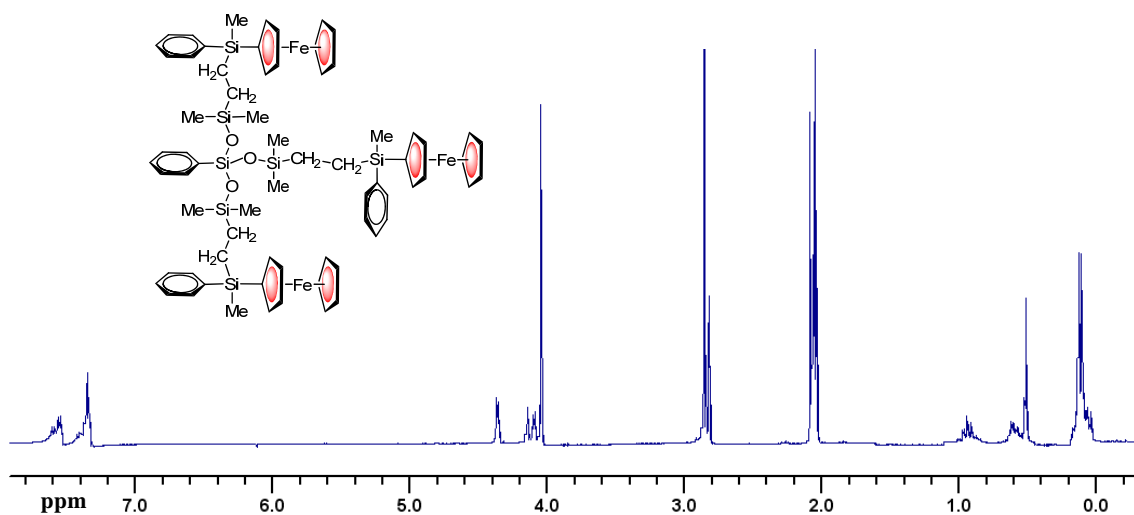


Figure S11. ^1H NMR spectrum (in $(\text{CD}_3)_2\text{CO}$, 300 MHz) of compound 7.

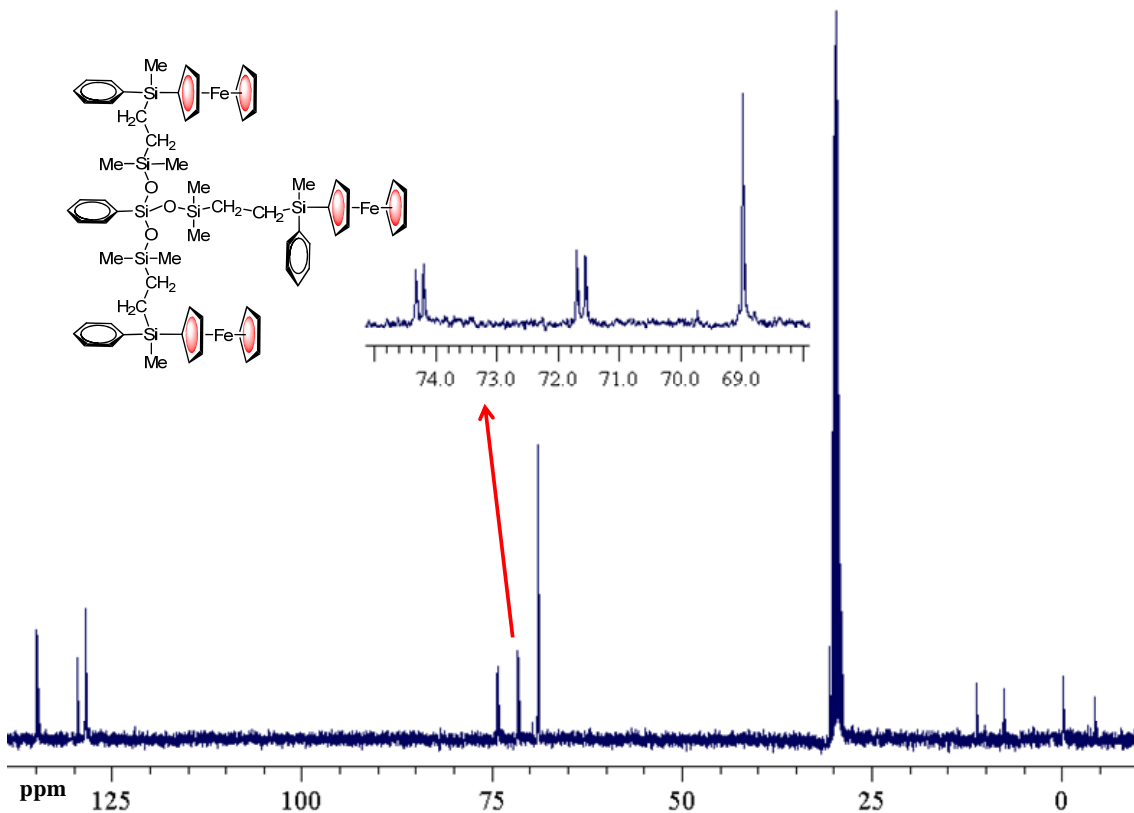


Figure S12. ^{13}C NMR spectrum (in $(\text{CD}_3)_2\text{CO}$, 75 MHz) of compound 7, (inset: expanded view of cyclopentadienyl region).

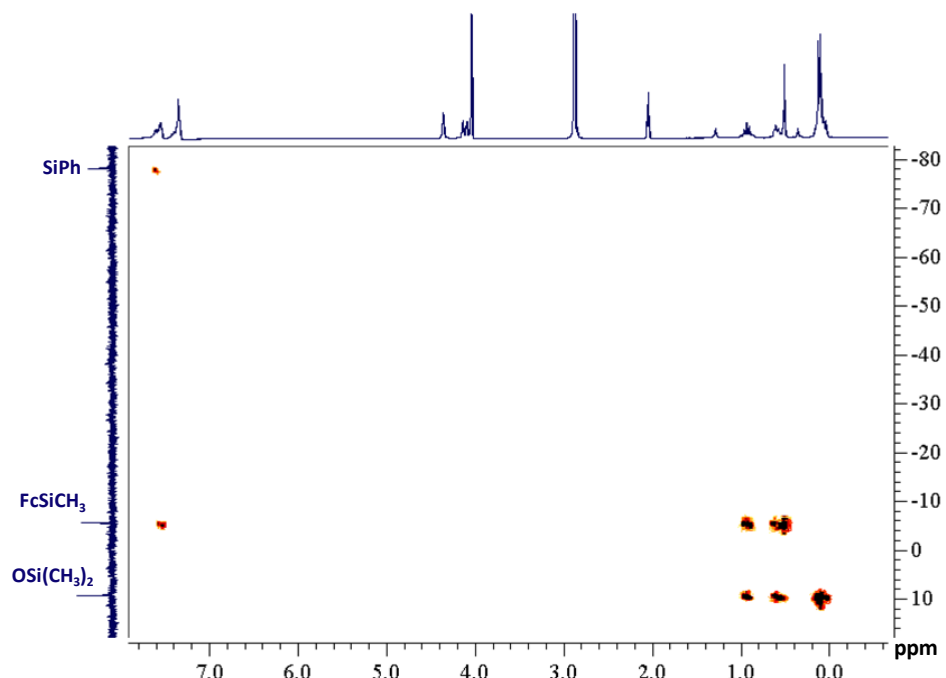


Figure S13. $\{^1\text{H}-^{29}\text{Si}\}$ HMBC spectrum (in $(\text{CD}_3)_2\text{CO}$, 300 MHz) of **7**.

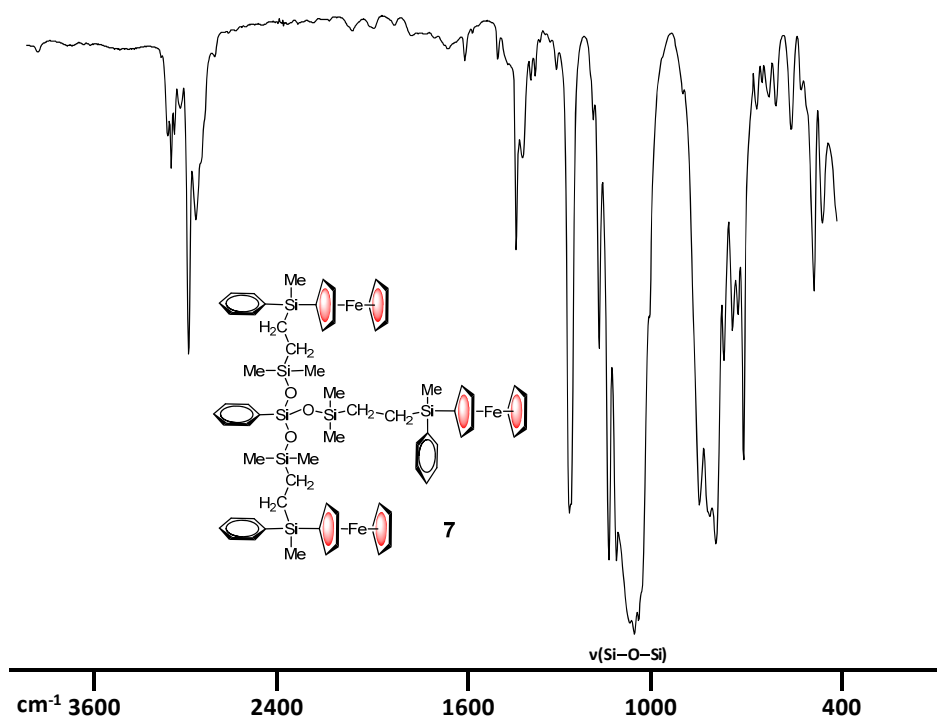


Figure S14. IR spectrum (in KBr windows) of compound **7**.

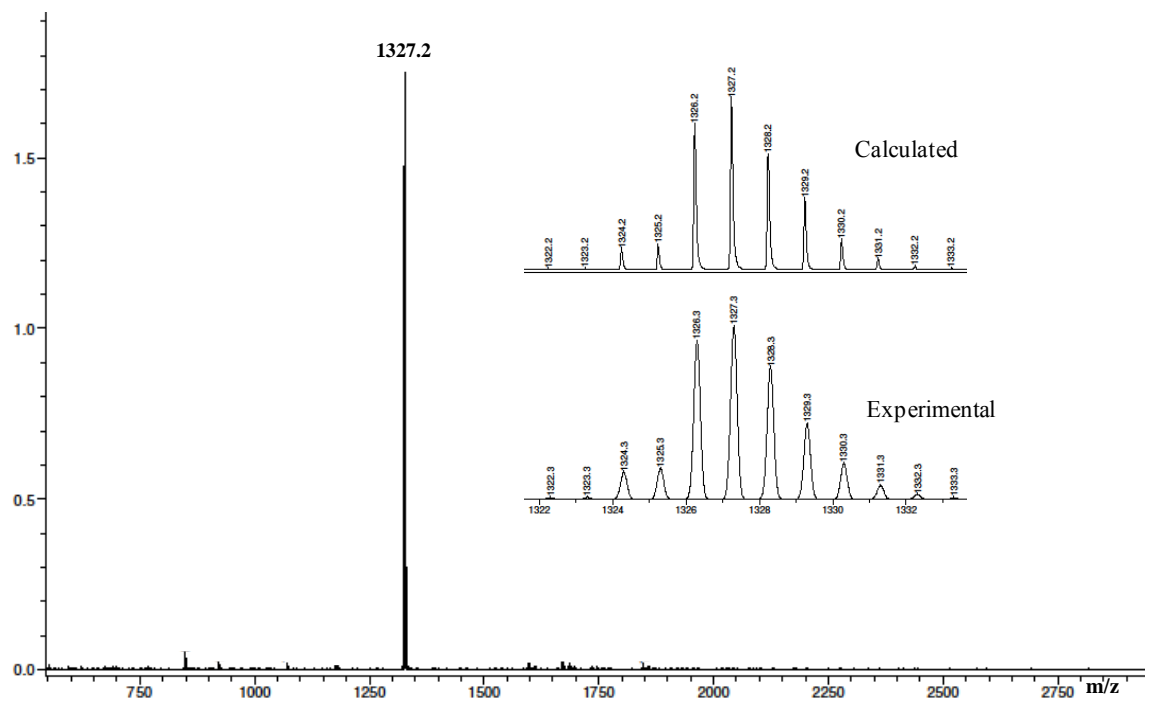


Figure S15. Mass spectrometry characterization by MALDI for compound 7. Inset: isotopic distribution of molecular ion peak of 7.

2.- Structural Characterization of Polymers 8–13

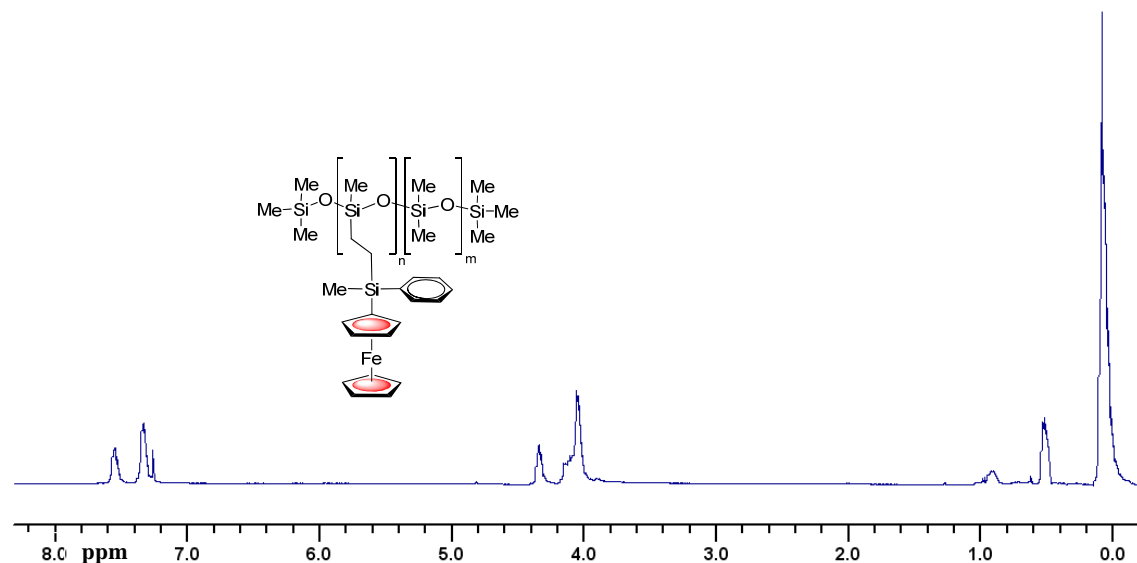


Figure S16. ¹H NMR spectrum (in CDCl₃, 300 MHz) of compound 8.

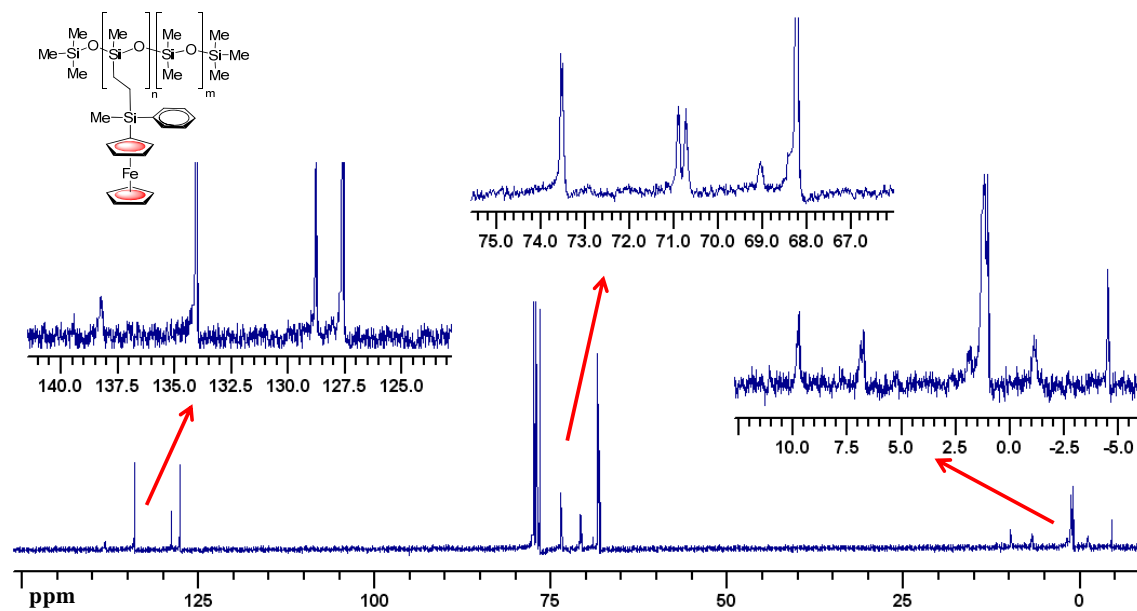


Figure S17. ¹³C NMR spectrum (in CDCl₃, 75 MHz) of compound 8, (inset: expanded view of phenyl, cyclopentadienyl, CH₂ and CH₃ regions).

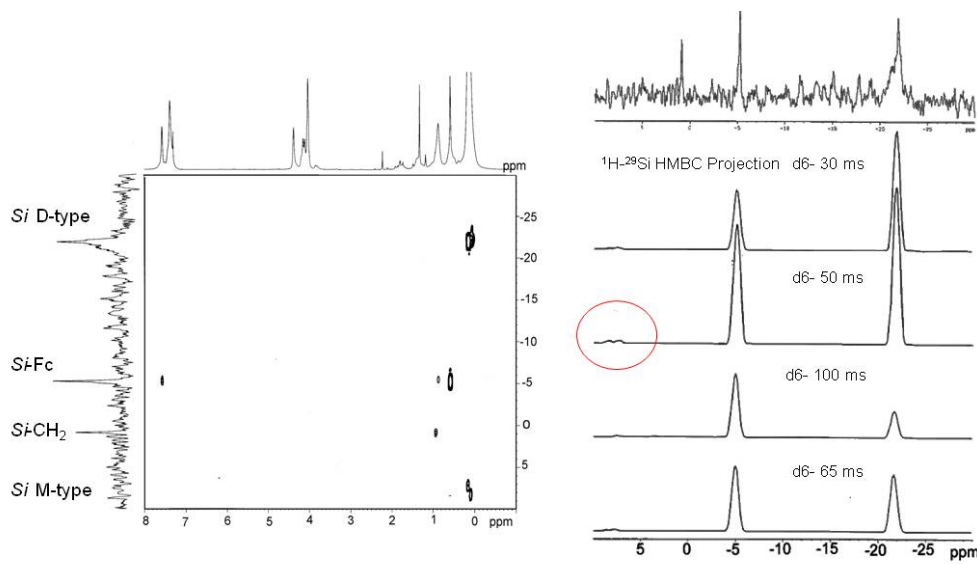


Figure S18. $\{^1\text{H}-^{29}\text{Si}\}$ HMBC spectrum (CDCl₃, 300 MHz) of **8** at $d = 50$ ms (left). Projections of $\{^1\text{H}-^{29}\text{Si}\}$ HMBC experiments at different d values (right).

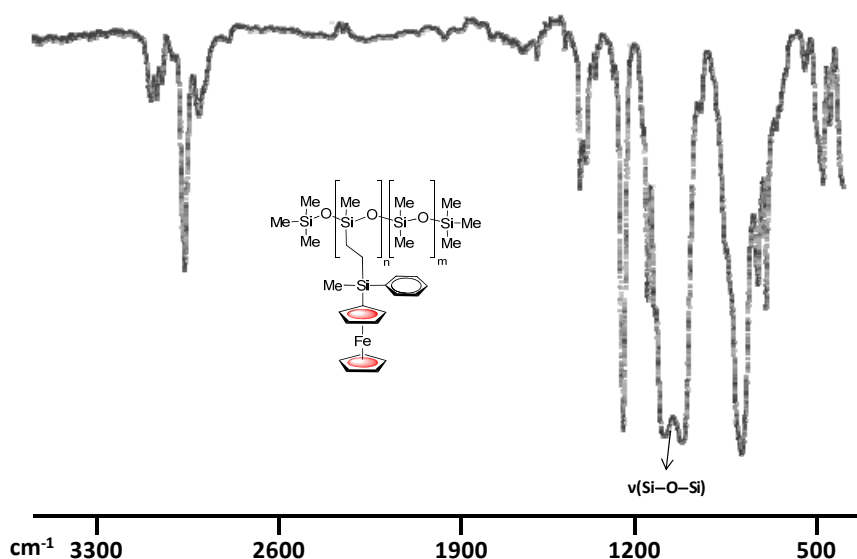


Figure S19. IR spectrum (in KBr windows) of compound **8**.

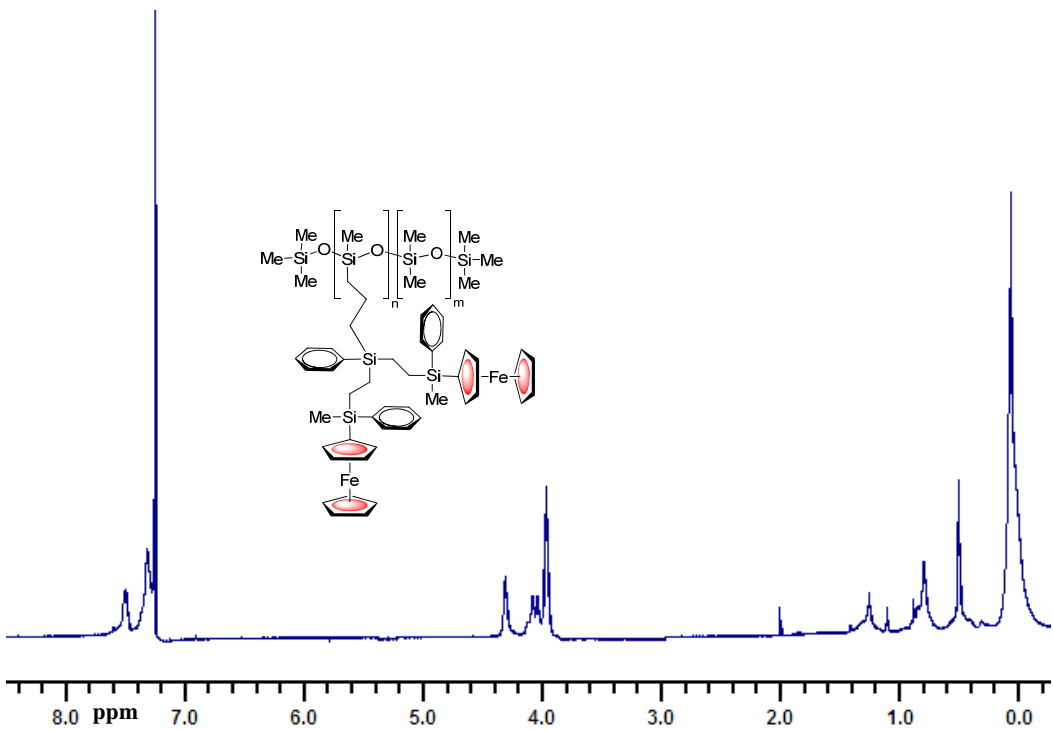


Figure S20. ¹H NMR spectrum (in CDCl₃, 300 MHz) of compound 9.

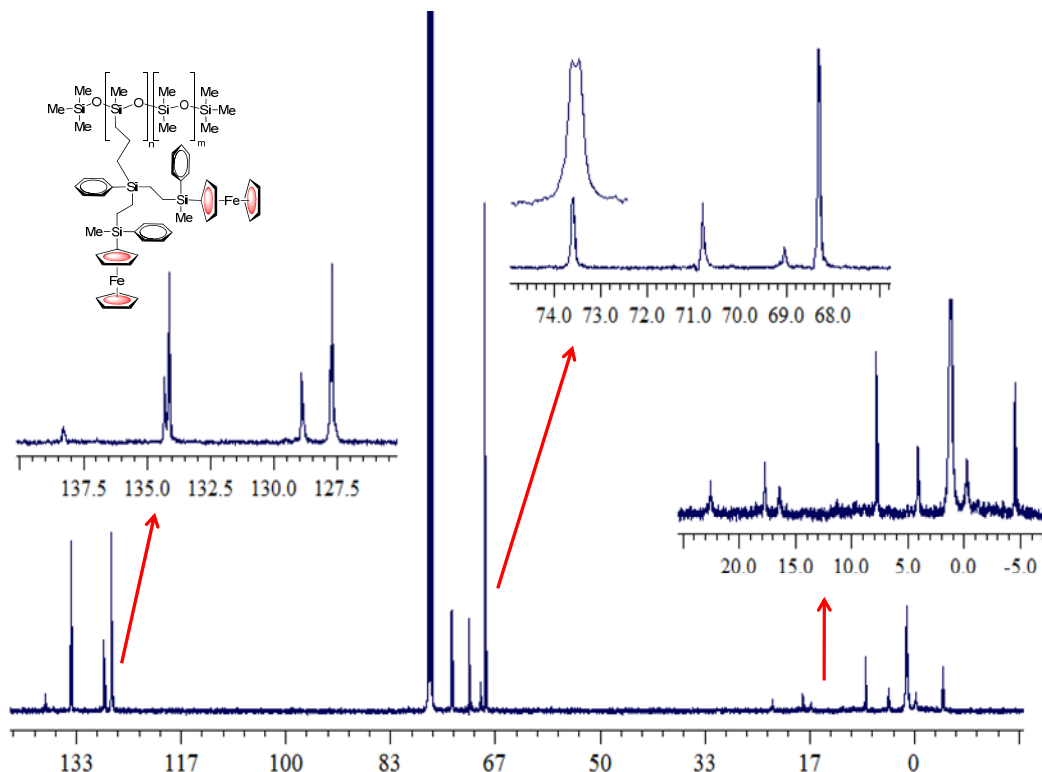


Figure S21. ¹³C NMR spectrum (in CDCl₃, 125 MHz) of compound 9, (inset: expanded view of phenyl, cyclopentadienyl, CH₂ and CH₃ regions).

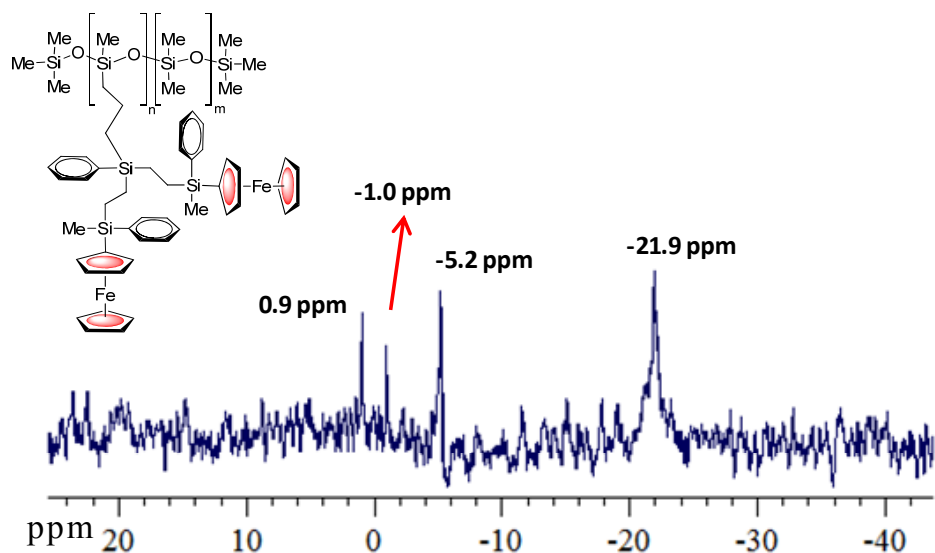


Figure S22. ^{29}Si NMR spectrum (in CDCl_3 , 99 MHz) of compound 9.

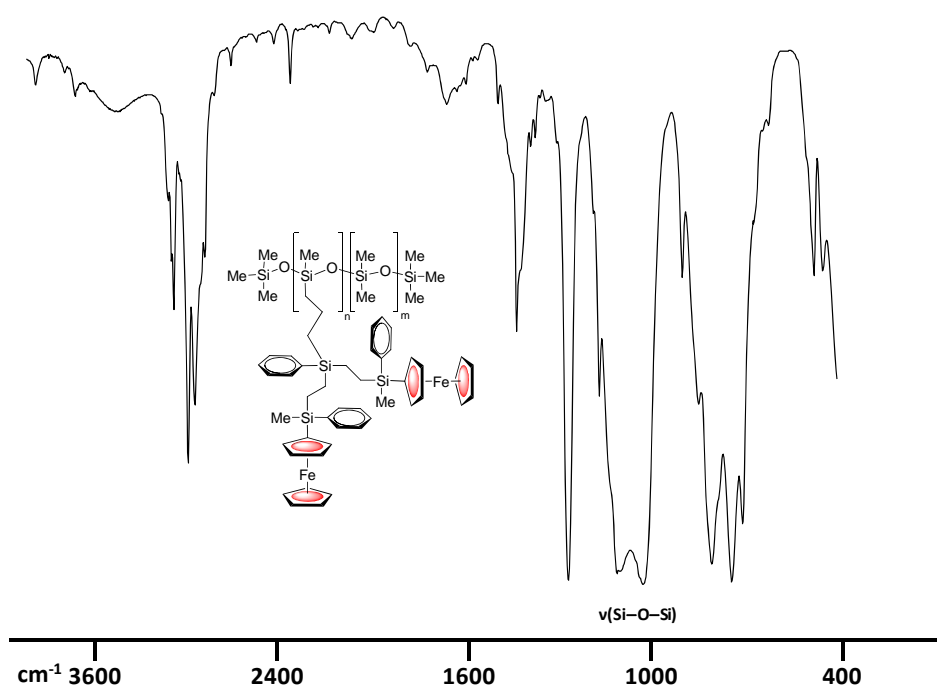


Figure S23. IR spectrum (in KBr windows) of compound 9.

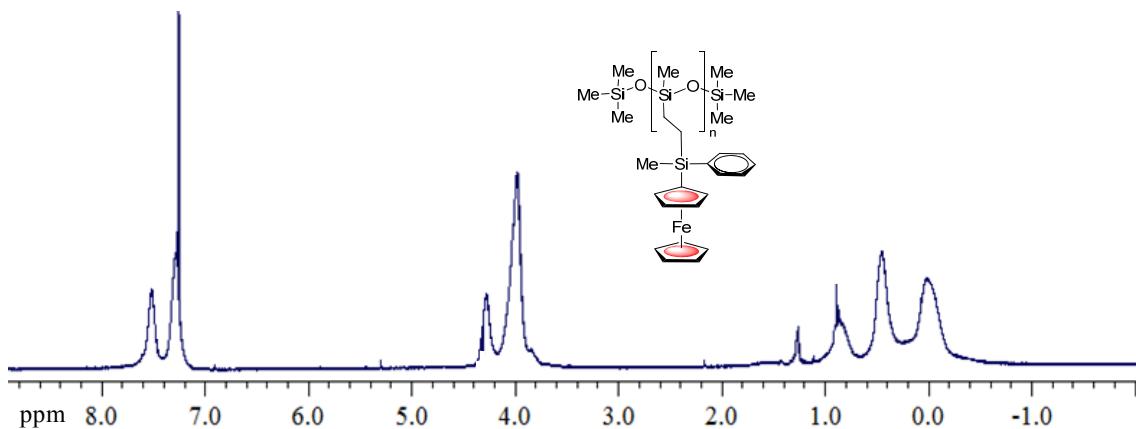


Figure S24. ^1H NMR spectrum (in CDCl_3 , 300 MHz) of compound **10**.

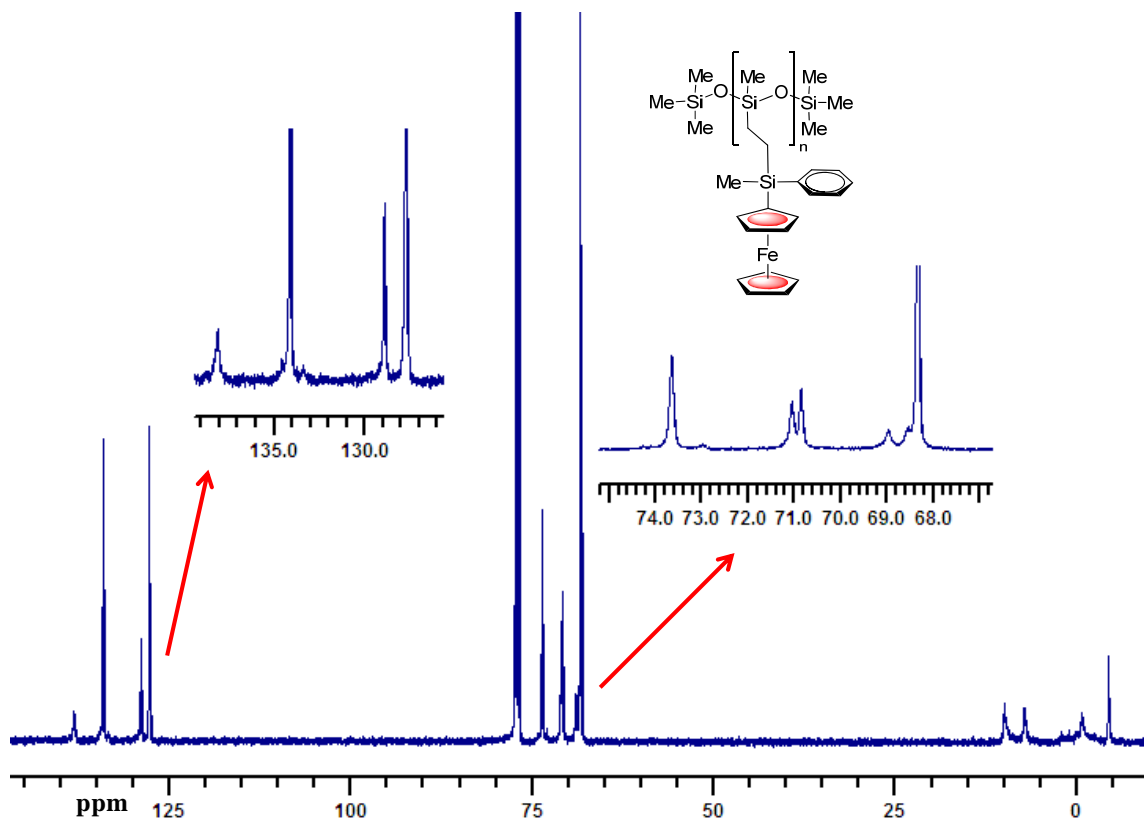


Figure S25. ^{13}C NMR spectrum (in CDCl_3 , 125 MHz) of compound **10**, (inset: expanded view of phenyl and cyclopentadienyl regions).

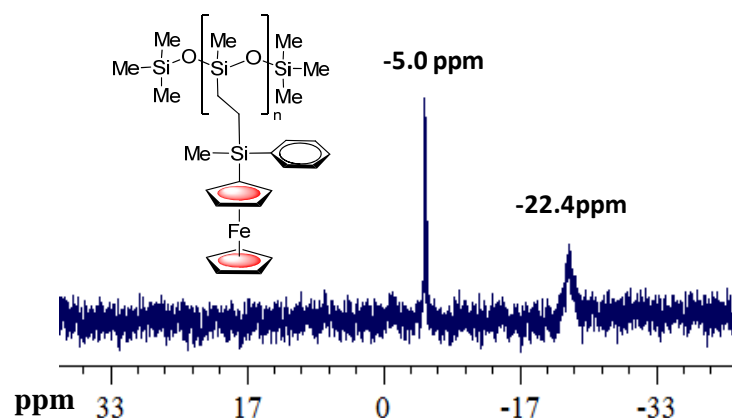


Figure S26. ²⁹Si NMR spectrum (in CDCl₃, 99 MHz) of compound **10**.

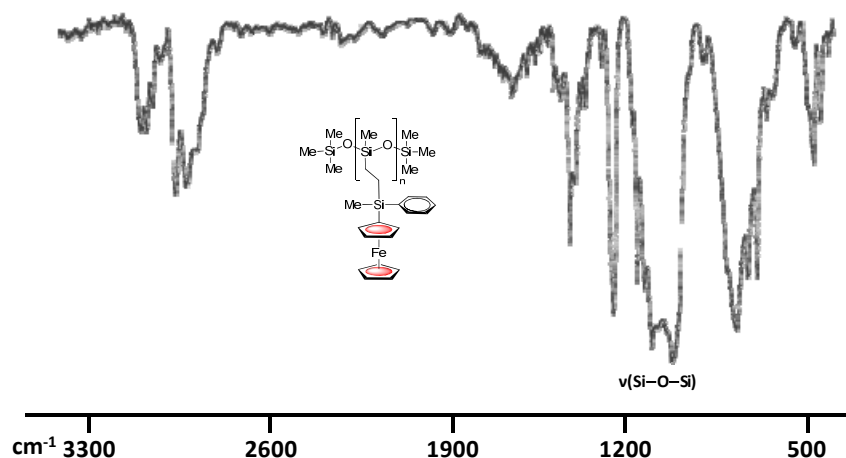


Figure S27. IR spectrum (in KBr windows) of compound **10**.

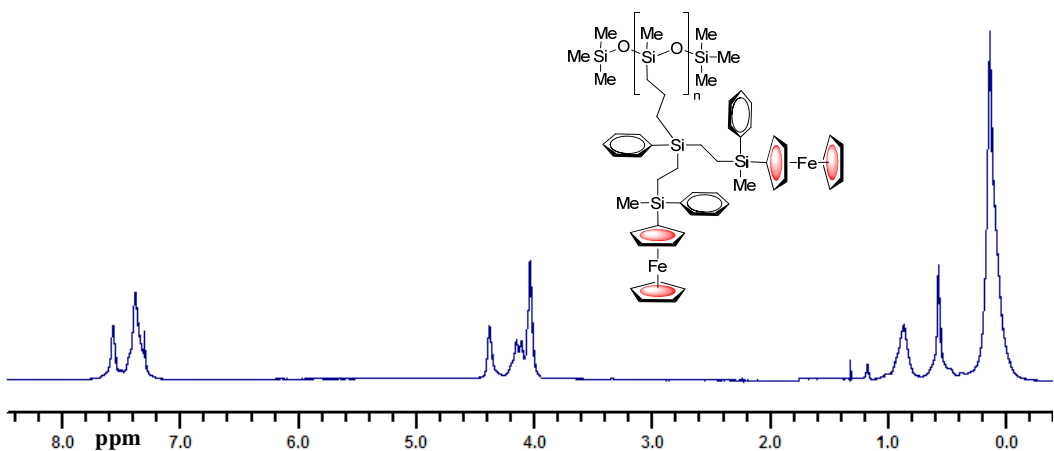


Figure S28. ¹H NMR spectrum (in CDCl₃, 300 MHz) of compound **11**.

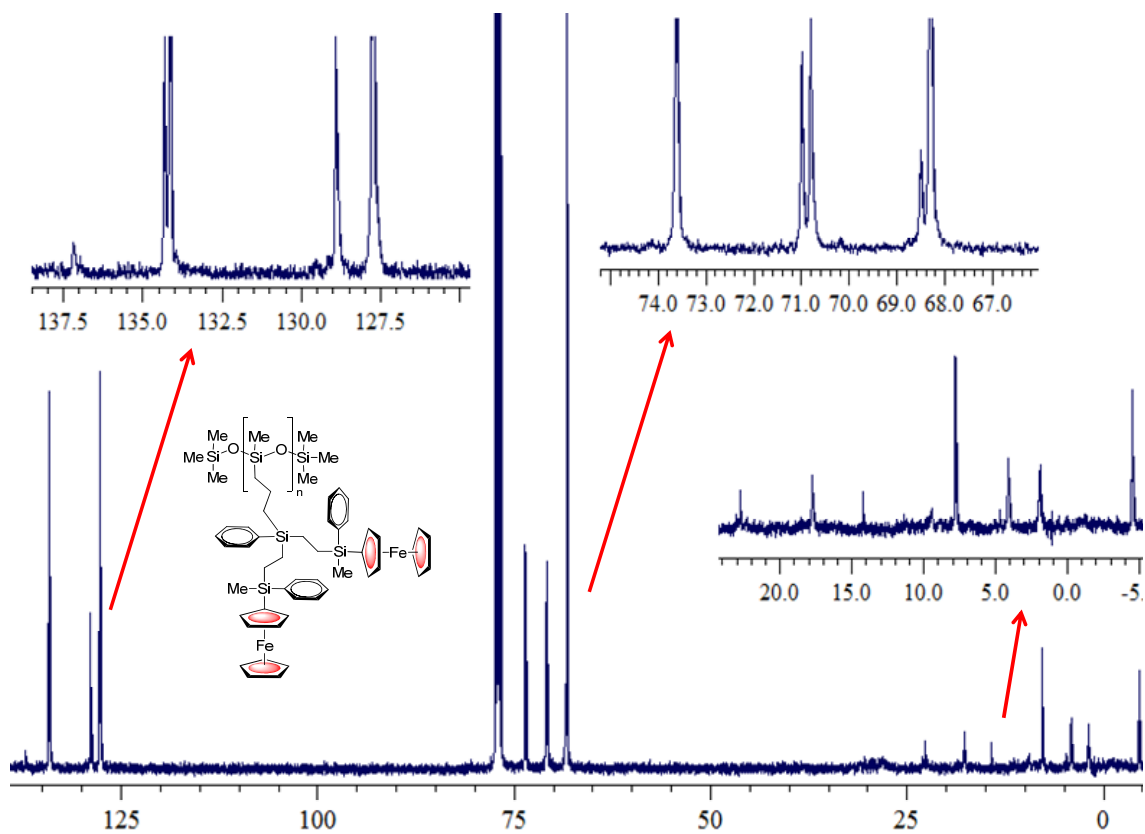


Figure S29. ¹³C NMR spectrum (in CDCl₃, 125 MHz) of compound **11**, (inset: expanded view of phenyl, cyclopentadienyl, CH₂ and CH₃ regions).

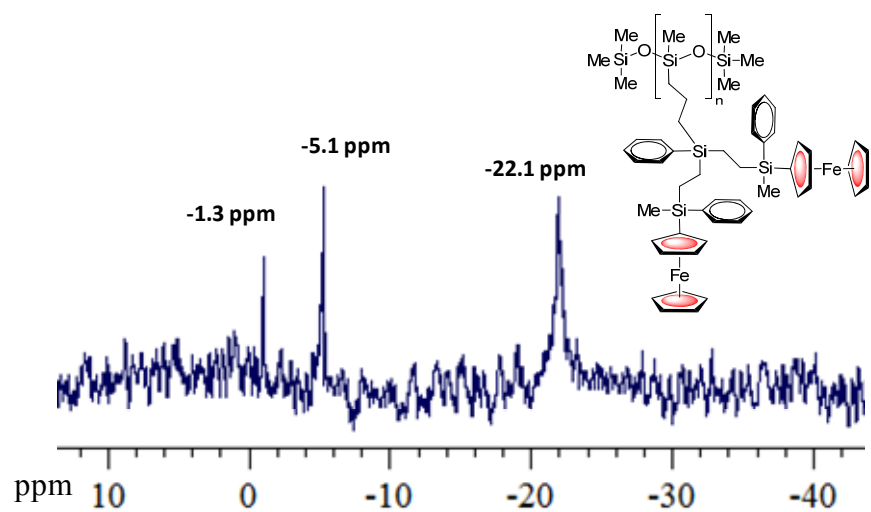


Figure S30. ^{29}Si NMR spectrum (in CDCl_3 , 99 MHz) of compound 11.

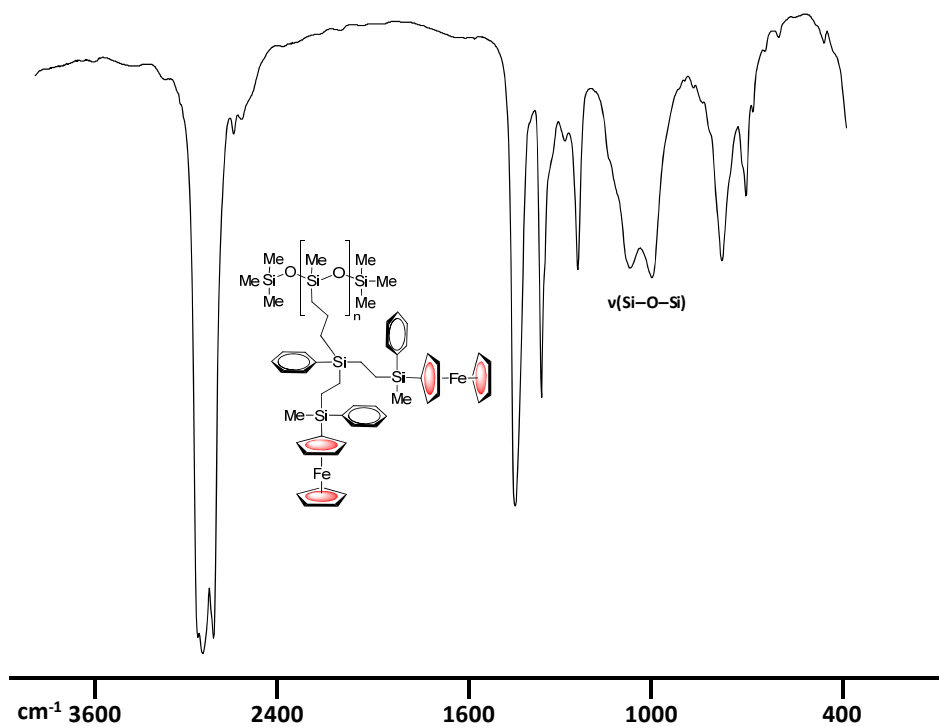


Figure S31. IR spectrum (in Nujol, KBr windows) of compound **11**.

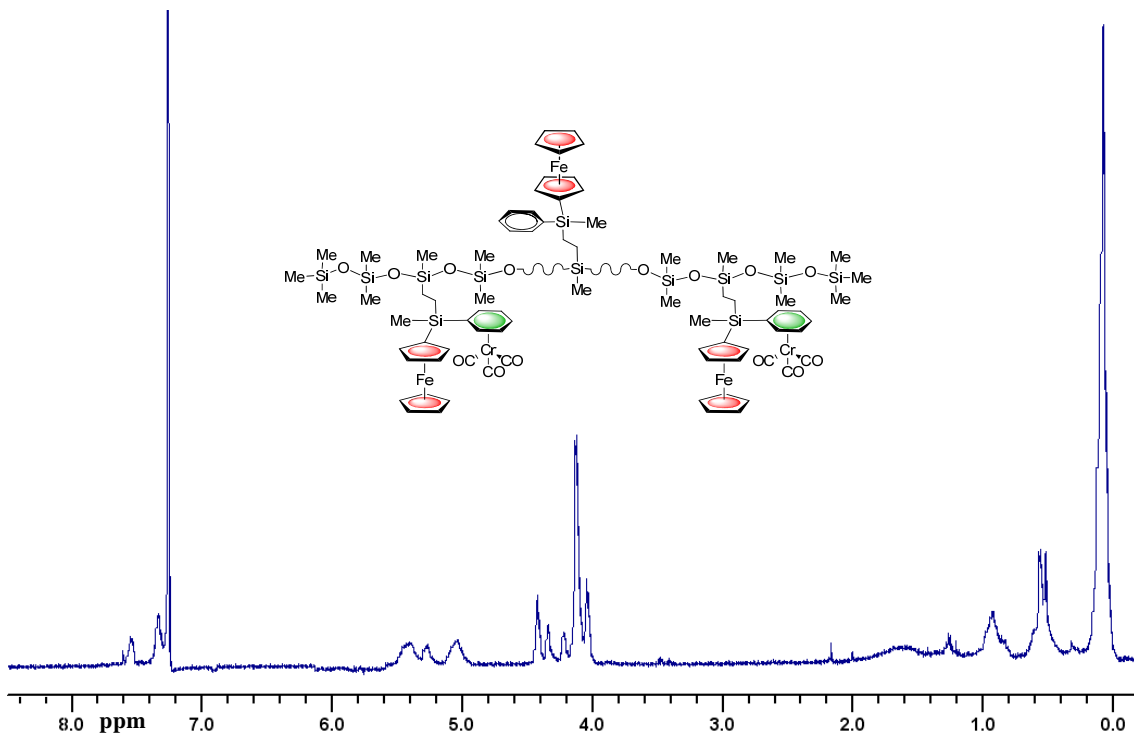


Figure S32. ¹H NMR spectrum (in CDCl₃, 300 MHz) of compound 12.

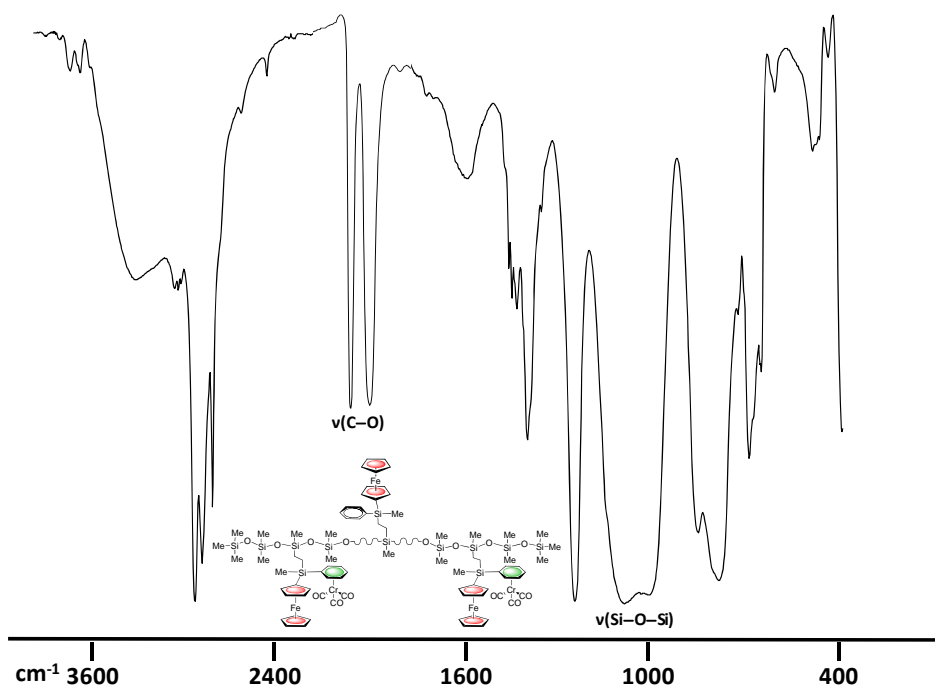


Figure S33. IR spectrum (in KBr windows) of compound 12.

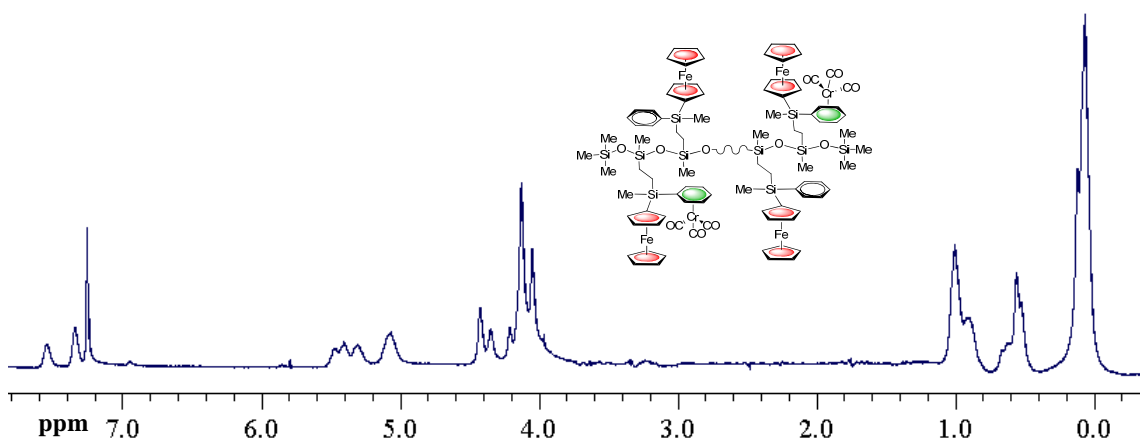


Figure S34. ^1H NMR spectrum (in CDCl_3 , 300 MHz) of compound **13**.

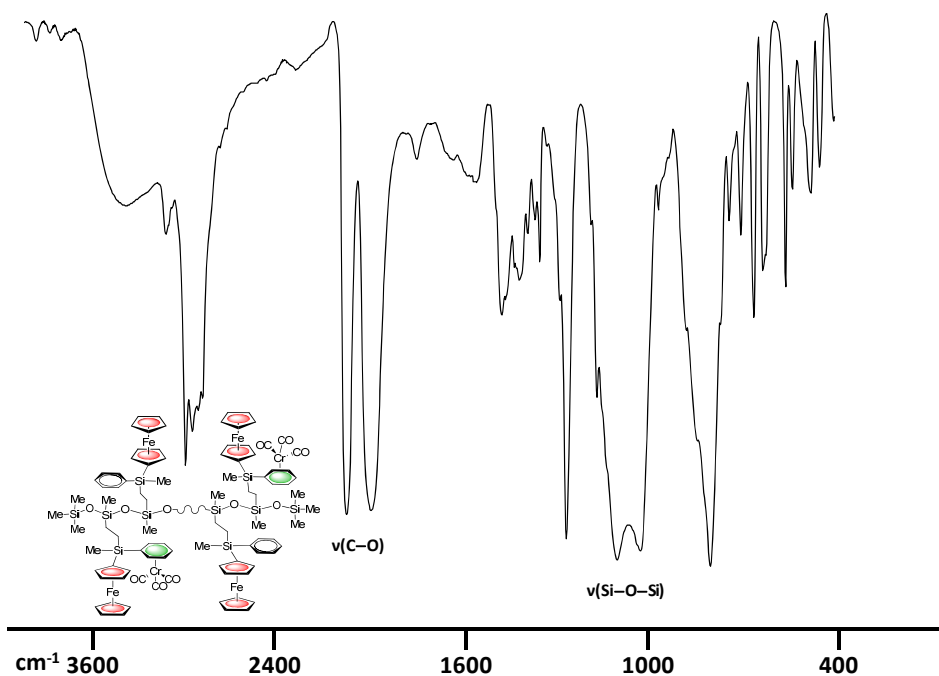


Figure S35. IR spectrum (in KBr windows) of compound **13**.

3.- Electrochemistry of Compounds 5–13.

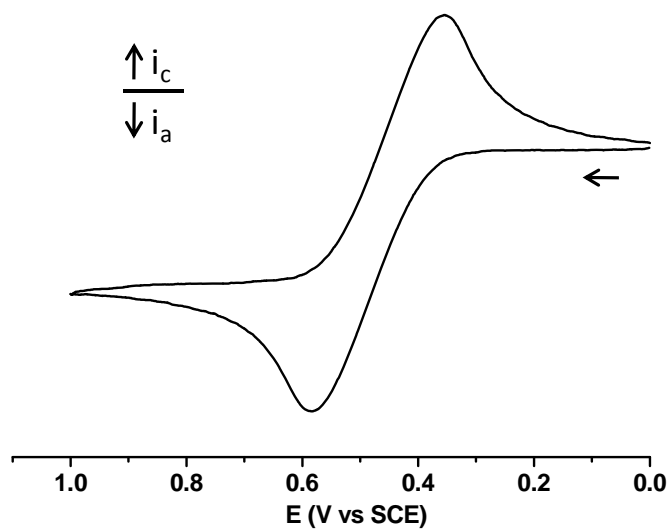


Figure S36. CV response of trimetallic **7** (10^{-3} M) recorded in CH_2Cl_2 containing 0.1 M Bu_4NPF_6 at a scan rate of 0.1 V s^{-1} .

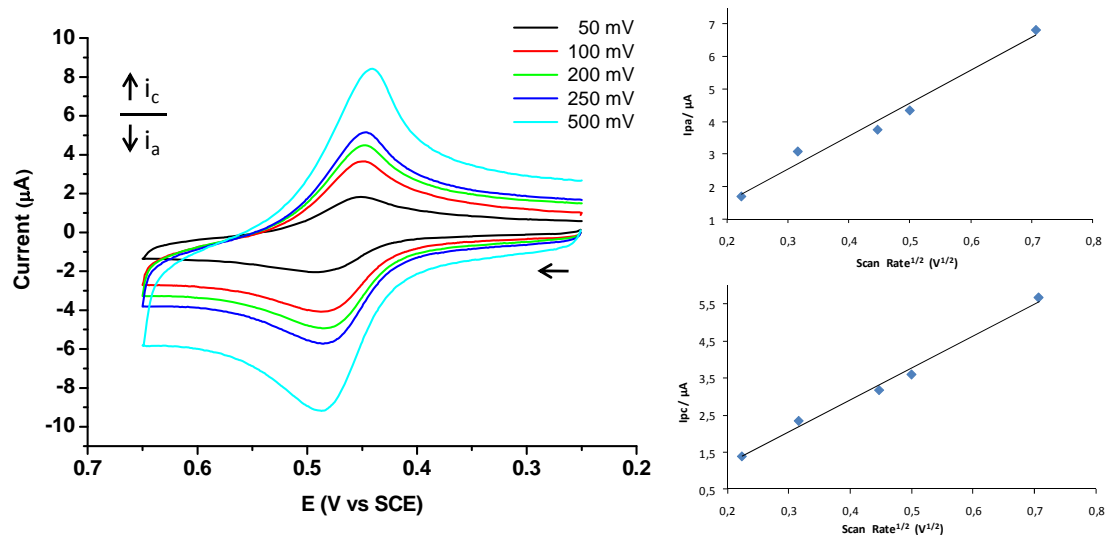


Figure S37. CV responses of ferrocenyl polysiloxane **8** (10^{-3} M) recorded in CH_2Cl_2 containing 0.1 M Bu_4NPF_6 , at different scan rates. Left: plots of I_{pa} and I_{pc} against scan rate $^{1/2}$.

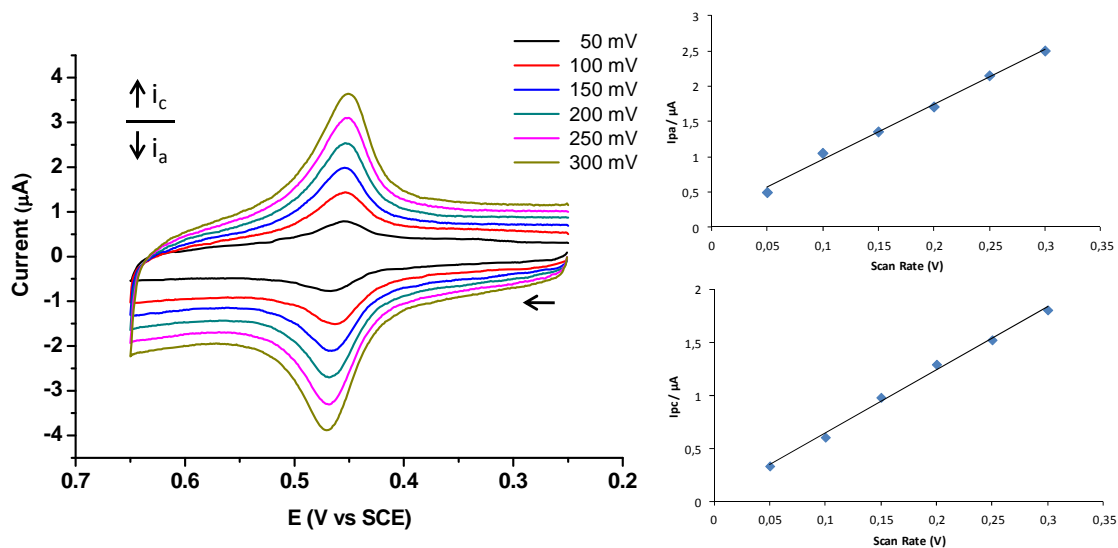


Figure S38. CV responses of a carbon-disk electrode modified with a film of ferrocenyl-containing dimethylsiloxane copolymer **8**, measured in 0.1 M $\text{Bu}_4\text{NPF}_6/\text{CH}_2\text{Cl}_2$ at different potential scan rates (mV s $^{-1}$). Left: Scan rate dependence upon the anodic and cathodic peak current.

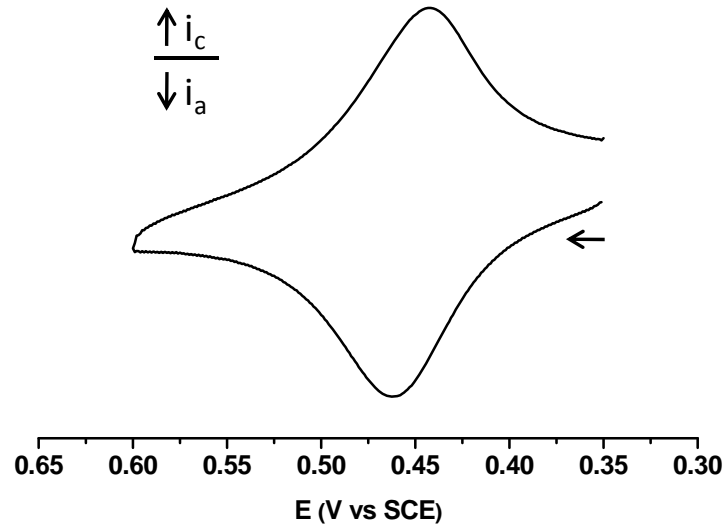


Figure S39. CV response (at 0.1 V s $^{-1}$) of a platinum-disk electrode modified with a film of ferrocenyl-containing dimethylsiloxane copolymer **9**, measured in 0.1 M $\text{Bu}_4\text{NPF}_6/\text{CH}_2\text{Cl}_2$.

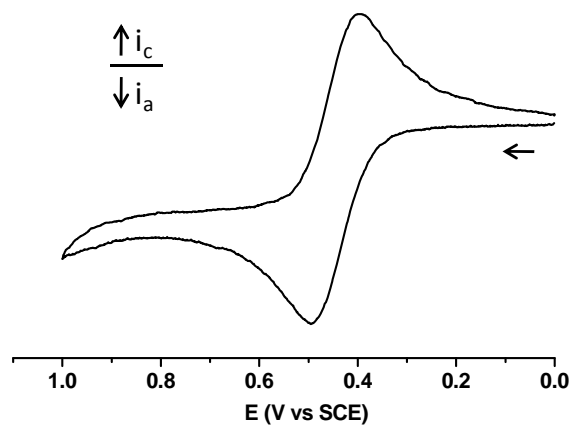


Figure S40. CV response of polysiloxane **11** (10^{-3} M) recorded in CH_2Cl_2 containing 0.1 M Bu_4NPF_6 .

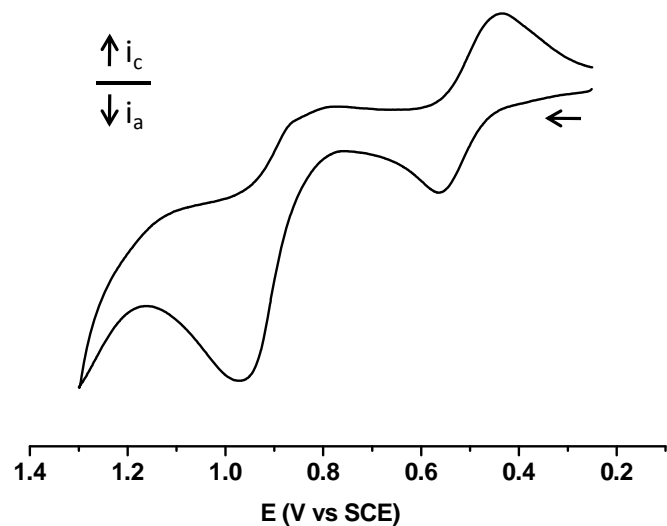
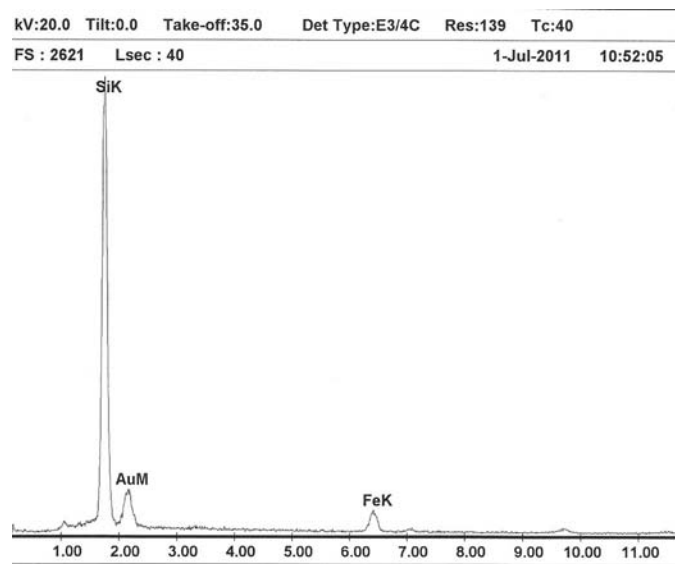


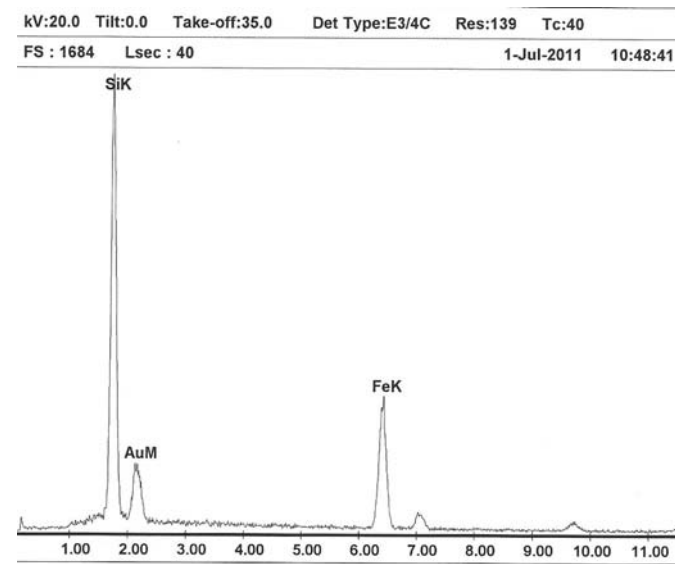
Figure S41. CV response of heterometallic polysiloxane **13** (10^{-3} M) recorded in CH_2Cl_2 containing 0.1 M Bu_4NPF_6 .

4.- Energy-dispersive X-ray (EDX) analyses of ceramic residues.



EDAX ZAF Quantification (Standardless)
 Element Normalized
 SEC Table : Default

Element	Wt %	At %	K-Ratio	Z	A	F
SiK	62.80	87.62	0.5168	1.0641	0.7733	1.0001
AuM	27.28	5.43	0.1476	0.7629	0.7091	1.0000
FeK	9.91	6.96	0.0913	0.9573	0.9516	1.0110
Total	100.00	100.00				



EDAX ZAF Quantification (Standardless)
 Element Normalized
 SEC Table : Default

Element	Wt %	At %	K-Ratio	Z	A	F
SiK	43.62	68.53	0.3036	1.0842	0.6418	1.0005
AuM	23.10	5.17	0.1355	0.7782	0.7540	1.0000
FeK	33.28	26.30	0.3148	0.9762	0.9607	1.0083
Total	100.00	100.00				

Figure S42. EDX analyses of the ceramic residue obtained by the pyrolysis of dendronized ferrocenyl polysiloxane **9** (at 1000°C under a nitrogen atmosphere), top: in the bulk; bottom: in the clusters of the surface.